Journal Pre-proof

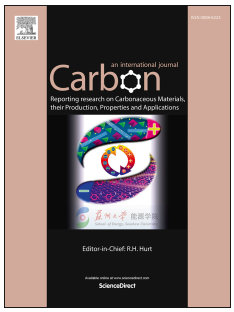

Ethylene-induced welding of single-walled carbon nanotube films to enhance mechanical and optoelectronic properties

Javier A. Ramirez B., Dmitry V. Krasnikov, Hassaan A. Butt, Veronika A. Dmitrieva, Svetlana I. Serebrennikova, Oleg R. Trepalin, Aliya R. Vildanova, Vladislav A. Kondrashov, Anastasia E. Goldt, Dmitry V. Dzhurinskiy, Julia A. Baimova, Rajath Alexander, Amit Kushal, Kinshuk Dasgupta, Omid Akhavan, Albert G. Nasibulin

PII: S0008-6223(25)00246-5

DOI: https://doi.org/10.1016/j.carbon.2025.120230

Reference: CARBON 120230

To appear in: *Carbon*

Received Date: 4 December 2024

Revised Date: 11 March 2025

Accepted Date: 14 March 2025

Please cite this article as: J.A. Ramirez B., D.V. Krasnikov, H.A. Butt, V.A. Dmitrieva, S.I. Serebrennikova, O.R. Trepalin, A.R. Vildanova, V.A. Kondrashov, A.E. Goldt, D.V. Dzhurinskiy, J.A. Baimova, R. Alexander, A. Kushal, K. Dasgupta, O. Akhavan, A.G. Nasibulin, Ethylene-induced welding of single-walled carbon nanotube films to enhance mechanical and optoelectronic properties, *Carbon*, https://doi.org/10.1016/j.carbon.2025.120230.

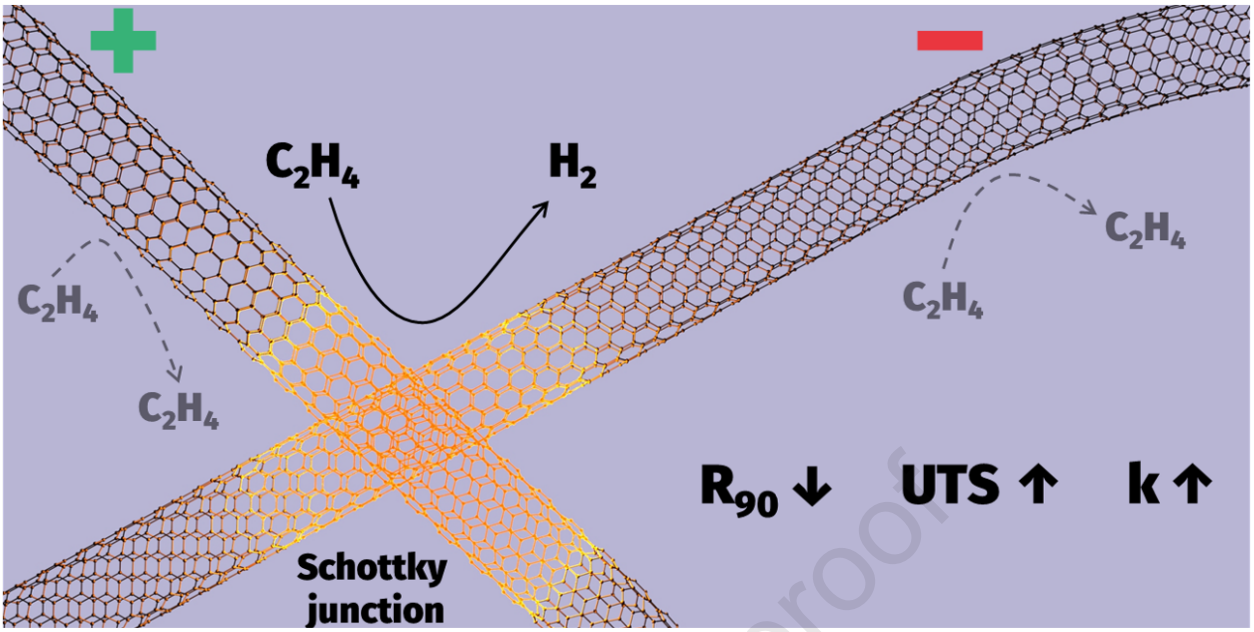

Ethylene-induced welding of single-walled carbon nanotube films to enhance mechanical and optoelectronic properties

*Javier A. Ramirez B.[1], Dmitry V. Krasnikov[1,] *, Hassaan A. Butt[1], Veronika A. Dmitrieva[1], Svetlana I. Serebrennikova[1], Oleg R. Trepalin[1,2], Aliya R. Vildanova[1], Vladislav A. Kondrashov[1], Anastasia E. Goldt[1], Dmitry V. Dzhurinskiy[1], Julia A. Baimova[3], Rajath Alexander[4], Amit Kushal[4], Kinshuk Dasgupta[4], Omid Akhavan[5], and Albert G. Nasibulin[1,] **

[1] Skolkovo Institute of Science and Technology, Nobelya str. 3, 121205, Moscow, Russia

[2] Dmitry Mendeleev University of Chemical Technology of Russia, Miusskaya sq., 9, 125047, Moscow, Russia

[3] Institute for Metals Superplasticity Problems of RAS, Khalturina 39, 450001, Ufa, Russia

[4] Bhabha Atomic Research Centre, 400085, Mumbai, India

[5] Department of Physics, Sharif University of Technology, P.O. Box 11155-9161, Tehran, Islamic Republic of Iran

AUTHOR INFORMATION

Corresponding Author

*E-mail: d.krasnikov@skol.tech *E-mail: a.nasibulin@skol.tech

ABSTRACT

Single-walled carbon nanotube (SWCNT) free-standing films combine high electrical conductivity with exceptional mechanical stability and optical transparency, opening the road for various applications: bolometers, thermophones, filters, *etc*. Here, we improve the performance of SWCNT free-standing films by engineering the intersections between the nanotube bundles –the building blocks forming and defining the conductivity and mechanical performance of the material. Hence, we propose a new, rapid, and scalable technology for the tailorable treatment of SWCNT free-standing films with ethylene (C_2H_4) under resistive heating. The technology comprises the high-temperature Joule heating of SWCNT free-standing films (700-1200 °C) combined with an exposure to ethylene flow at a pressure below 0.3 mPa, with an energy consumption as low as *ca.* 10 W/cm^2. Using a set of methods (UV-vis-NIR and Raman spectroscopies, scanning and transmission electron microscopies, four-probe sheet resistance, temperature coefficient of resistance, and combined ultimate tensile strength/gauge factor measurements) combined with molecular dynamics simulations, we observe the film welding, *i.e.*, the deposition of sp^2 carbon coating presumably on nanotube bundle junctions. We show the welded free-standing films to enhance the performance of the filters and transparent electrodes (after doping with $HAuCl_4$), strengthening the material up to an order of magnitude (ultimate tensile strength ~ 22 MPa) and reaching one of the state-of-the-art performance values of 30 Ohm/sq at a transmittance of 90 % at 550 nm (electrical conductivity ~ 30,000 S/cm).

KEYWORDS: single-walled carbon nanotubes; membranes; welding; molecular dynamics; transparent electrode; ethylene pyrolysis

1. INTRODUCTION

Carbon nanotubes occupied one of the major shares of nanotechnology research[1], relying not only on a remarkable set of mechanical, optical, and electronic features[2–5], but also on a variety of the morphology forms accessible: powder, forest, fiber, film, aerogel, individual object, *etc.* [6] Free-standing films are a specific case of carbon nanotube assembly usually produced by filtration of nanotube dispersions (buckypaper; usual thickness > 200 nm) [7,8] or with the aerosol CVD method (free-standing films; thickness < 1 μm) [9–11]. Carbon nanotube free-standing films are considered to be promising for numerous applications, each of them relying on a specific set of properties. For example, the combination of high mechanical strength and fibrous morphology allows them to pursue protective membranes: aerosol filters and EUV pellicles [12–15]. The role of junctions in overall conductivity combined with availability for p- and n-type doping defines the free-standing films as a promising sensor [16,17], transparent electrode[18,19], or thermoelectric generator[20,21]. A variety of applications relies on a combination of high surface area, mechanical and chemical stability, as well as prominent electrical conductivity: supercapacitors[22], cathodes and anodes for batteries[23,24], substrates for electrocatalysis[25,26], thermophones[27,28], infrared bolometers[29,30], Joule heaters[31,32], and regeneration units[33]. Moreover, the free-standing films can contribute to new emerging fields: carbon dioxide capture membranes [34], THz devices[35–37], and biology scaffolds[38,39].

To improve the free-standing film performance, a balance between the features of individual nanotubes and membrane macrostructure is crucial. Optimization of material features during both synthesis[40] and post-processing[41], as well as either for individual nanotubes[42–44] or a part of, for example, a film[45,46], is a broad topic covered by various groups. At the same time, the

number of publications on tuning the membrane properties is substantially lower, opening a wide window for further improvement. As most applications rely on the mechanical and electronic properties of the free-standing films, the direct engineering of the nanotube junctions – the very point defining the overall membrane conductivity and strength – highlights the avenue for development. On the one hand, the nanotube junctions can be restructured to obtain a single joint object; such an object was numerously discussed to have advanced strength[47] and obtained by means of plasma[48], laser[49], or electron beam [50]welding as well as high-pressure processing. On the other hand, the junctions can be coated with a media or another carbon-based species to provide a "glue-like" effect [51,52]. Such a coating has been widely shown to affect the mechanical properties[53] and conductivity of the junction[54,55]. Nevertheless, as a rule, the coating uniformly covers the film, altering the absorbance and mass of the unit – the crucial parameters for, for example, thermophones, extreme ultraviolet pellicles, and transparent electrodes.

In this work, we propose a novel strategy to modify the junctions between the nanotubes employing one of their key features – high resistance. We use Joule (resistive) heating to locally overheat the junctions in ethylene-containing media to stimulate spatially non-uniform pyrolysis to create lateral carbon deposits on the tube-tube Schottky barriers or the whole film by the carbon lamella formation, depending on the treatment time. In this sense, we are the first to perform chemical reactions on a resistively heated SWCNT free-standing films. Indeed, the previous works on resistive heating of freestanding films were devoted to surface and volume cleaning by physical evaporation for IR or EUV applications [33,56]. Here, we examine the characteristics of such nanotube free-standing films in terms of defective structure, transparency, and conductivity by employing a set of spectroscopic, microscopy, and electrical methods combined with molecular dynamics simulations. We show the welded free-standing films to have increased mechanical and

improved optoelectronic characteristics that ensure the advanced performance of nanotube-based filters and transparent electrodes.

2. MATERIALS AND METHODS

The single-walled carbon nanotubes (SWCNTs) were prepared by aerosol (floating catalyst) CVD method based on the Boudouard reaction (CO disproportionation). A catalyst precursor (ferrocene, Sigma Aldrich, 98%) was vaporized and transferred in a tubular quartz reactor for decomposition at temperatures higher than 400 °C in CO/CO_2 atmosphere (99.99% CO, 99.995% CO_2) to form an aerosol of Fe-based nanoparticles. The catalytic CO disproportionation at 850 °C results in the growth of carbon nanotubes. The addition of CO_2 is known to tune the diameters of SWCNTs, and in our research we used two types of nanotubes [45]. For structural and mechanical analysis, we employed SWCNTs with an average diameter of about 2 nm, while for transparent electrode applications we chosen nanotubes with average diameter of 1.4 nm due to lower sheet resistance of the thin films [45]. A randomly oriented SWCNT network was collected on a nitrocellulose filter (HAWP, Merck Millipore, USA). The SWCNT film was picked from the filter using cylindrical stainless-steel electrodes (304L stainless steel tube with a diameter of 0.8 mm) by the dry transfer technique [57] to obtain a free-standing film. The SWCNT free-standing films were purified from Fe catalyst with Joule (resistive) heating for 3 minutes at 1400 °C according to the procedure reported in [56].

The welding treatment is to be applied in a vacuum chamber (Figure S1) ($P \leq 0.3$ mPa), using a Pfeiffer hi-cube 80 vacuum station (Germany) with two vacuum gauges (Pfeiffer MPT100, Germany cold cathode and Pirani, Thyracont Vacuum instruments GmBH) discussed in detail previously [56]. Pressure-regulated ethylene (C_2H_4; 99.9 %) was fed to a mass flow controller

(Alicat, USA) to a nozzle inside the chamber at a rate of 1 sccm (no carrier gas was used; the pressure within the chamber was still of ≤ 0.3 mPa). The flow of ethylene passed through the SWCNT free-standing film while heated, as shown in Figure S1. The film was heated in a single step by direct current (DC) with a power source Electro Automatics 3200-04C (Germany). The temperature was controlled with a pyrometer (Euromix RXR 2300, Russia) in the range from 700 to 1700 °C based on spectral response from 1.0 to 1.6 μm. A detailed description of the calibration procedure for the pyrometer is described elsewhere [56]. Briefly, the calibration of the pyrometer used for SWCNT free-standing film temperature estimation was made by direct comparison of two different thermocouples in direct contact with the SWCNT free-standing films, in a specially designed holder. The presence of a borosilicate window to separate the atmosphere from the low-pressure chamber makes impossible to directly compare atmospheric pressure measurements with low pressure; the homogeneity of the windows affects directly the precise estimation of the film emissivity at low pressure. For this purpose, the measurements were taken in 9 points around the center of the window, to understand if there was a meaningful affectation of the measured temperature. A specially designed thermocouple amplifier was placed inside of the low-pressure chamber to avoid introducing additional errors by extending thermocouple wires. By trial and error, 10 measurements of a correct emissivity value were found that allowed us to keep temperature deviation between instruments of no more than 1%. The emissivity value was found to be 0.10.

The optimum flow rate was empirically determined to be < 5 sccm. No changes were observed below 0.1 sccm (the minimum flow acceptable for the MFC used). Flowrates higher than five sccm tend to cause sample deformation and breakage at high temperatures.

To assess the thickness and density of pristine SWCNT films, we employed the results of the recent study by Ermolaev *et al.*[58], where a combination of SEM, AFM, and ellipsometry allowed to deduce a Beer-Lambert law-like relation between the optical absorbance at 550 nm (A_{550}) for SWCNT thickness (h [nm] = 239·A_{550}). BM 22-G analytical balances (AND, Japan) were employed to study the film mass with a precision of up to 1 μg. The film thickness and area allowed us to estimate the bulk density. Nevertheless, as the mass of each sample with a thickness of 200 nm is around 30 μg, it gave the bulk density of 1.6 ±0.5 mg/cm^3. It should be noted that for the treated films the absorbance study of the thickness is not relevant; thus, we considered the film thickness to be the same, while the mass change is proportional to changes in absorbance as Fe catalyst residuals do not play a significant role in visible range[56].

Resistivity measurements of the pristine and treated free-standing films were performed by using a Jandel RM3000 four-probe station, with the SWCNTs transferred onto quartz substrates. for the applications of transparent conducting films, the sheet resistance is the most abundant [59]. In order to facilitate data comparison with other relevant publications, we wish to remain with the sheet resistance, R_s and equivalent sheet resistance, R_{90}, which allows one to compare different materials with different thicknesses and absorbance and is widely employed as the key performance indicator for transparent electrodes [59–61]. We also duplicate the data as electrical conductivity to enhance the relevance for applications usually dealing with this descriptor (fiber technologies, thermoelectrics, composites, *etc.*). Treated and pristine free-standing films were transferred to fused silica quartz substrates of 9x12 mm^2 on which bilateral simultaneous doping by $HAuCl_4$ was performed following the guidelines from [62]. Doping was carried out using a 30 mM $HAuCl_4$ dopant solution by drop casting technique with a 7 μl dose. 30 mM dopant solution was prepared by dissolving of required amount of $HAuCl_4$*$3H_2O$ in pure ethanol. After doping,

the samples were dried at ambient conditions until the isopropyl alcohol had completely evaporated.

To assess the SWCNT thin film thickness, both pristine and welded films were dry transferred onto smooth Si/SiO_2 substrates, after which a microtome blade was used to create a small cut along the sample. This cut served as the point where baseline measurements started, and allowed the thickness of the films to be measured from there edges till a normalization point at their maximum thickness. A Bruker Multimode V8 atomic force microscope was used for thickness measurements in Quantitative NanoMechanical Mapping PeakForce tapping mode. A probe with a 3 N/m force constant (k) and reflective gold coating, with a scan rate of 0.2 Hz and a setpoint force of 10 nN was used. Imaging was performed at 512 × 512 resolution with the scan size of 5 x 20 μm^2, ensuring high accuracy. Preprocessing included plane leveling and line-wise offset correction to remove artifacts and enhance data reliability by Gwyddion.

The temperature dependence of the resistance was performed by a four-probe technique in the region from 100 K to 450 K. The resistance was measured with Keysight 34972A LXI Data Acquisition/Switch Unit (Keysight Technologies, Inc. USA) and the temperature control was provided with Linkam THMS350 Stage chamber under pressure of 0.1 bar with the rate temperature change of 10 °C/min.

Optical spectroscopy measurements were performed using Perkin Elmer Lambda 1050 UV-vis-NIR spectrometer in the range of 200 – 2400 nm with a resolution of 3 nm. Thermo Scientific DXRxi Raman Imaging microscope with a laser excitation wavelength of 532 nm was used for Raman spectroscopy measurements. The Raman spectra were normalized to G mode intensity.

The free-standing films were transferred on a TEM lacey Cu-300 grid and observed with an FEI Tecnai G2 F30 transmission electron microscope. To decrease the role of carbon nanotube destruction under the beam, we focused the TEM at one position and then swiftly moved by a few hundred nm to find a new "untouched" spot and capture an image. To avoid SWCNT degradation under the electron beam, the images shown were captured at the very first moments of the spot observation (for this, we focused on one position and then swiftly moved by a few hundred nm to find a new "untouched" spot and capture an image). For SEM examination, freestanding samples were placed with their holders on aluminium support with carbon tape and observed using Helios G4 PFIB (ThermoFisher Scientific) scanning electron microscope.

Free-standing pristine and ethylene welded were evaluated on an universal testing machine and used as particle filters while recording the changes in differential pressure to understand the ultimate breakage pressure to extend the lifetime and endurance of welded SWCNT filters [61]. To compare and validate the mechanical property characterization conducted with the penetration testing technique, tensile testing of SWCNT thin films was performed using an Instron 5969 Universal Testing Machine with a 10 N load cell and 50 N pneumatic grips in constant crosshead speed of 0.1 mm/min. The films were attached to specialized holders, as shown in Figure S2. Films were dry-transferred onto the holders over the gauge length section, and held in place using silver conductive adhesive. The adhesive served a secondary purpose, allowing piezoresistive measurements during the tests (not provided here). Initial analysis determined that no unique stress-strain features needed to be highlighted until 0.01 strain, and the remaining samples were tested at a speed of 0.25 mm/min. Strain measurements were processed with VIC-2D Digital Image Correlation (DIC) software.

3. RESULTS AND DISCUSSION

3.1 Welding of SWCNT free-standing film

The SWCNT free-standing films were prepared by a combination of the aerosol CVD method [63] with the dry transfer technique [57]. To avoid possible catalytic decomposition of C_2H_4, we removed catalyst remains using the dry Joule heating procedure reported recently (3 min; 1400 °C) [56]; the purified films obtained are denoted hereinafter as "pristine free-standing films".

The free-standing film welding was performed in a low-pressure chamber (< 0.3 mPa) equipped with a mass-flow controller and a pyrometer (Figure 1a) to record the temperature of the resistively heated SWCNT free-standing film (Figure 1b). The design of a chamber, as well as pyrometer calibration, were discussed elsewhere [33,56]. Low pressure diminishes the convection effects discussed elsewhere[56]. It should be stressed that the pyrometer collects an integral signal from an area of 0.3 cm^2. As the average length of SWCNTs produced is *ca*. 10 μm [64], we expect most of the collected signal to come not from the junctions but from SWCNT bundles, while the temperature of the junctions is presumably higher.

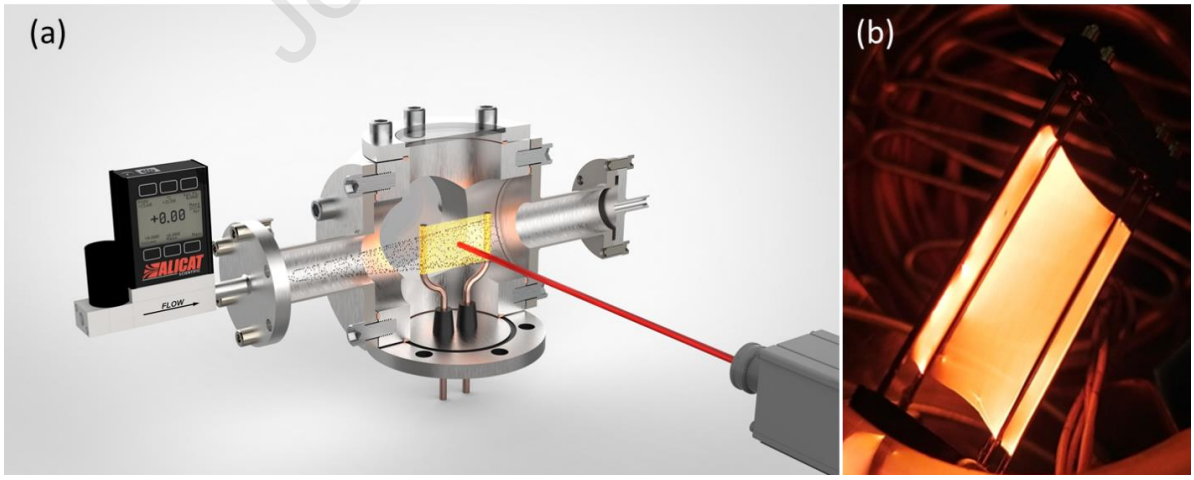

Figure 1. Schematic representation of the ethylene treatment reactor (a) and a photo of a resistively-heated SWCNT free-standing film at low pressure (b); a characteristic glowing of a free-standing film appears at a temperature > 600 ºC.

To assess the treatment effect on the film thickness, we employed atomic force microscopy with thick SWCNT films (T_{550}~25 %) to observe the effect with higher accuracy. Figure 2 (a) shows typical AFM scans the pristine SWCNT film, whereas Figure 2 (b) shows a SWCNT film which has been welded excessively (5 minutes at 1100 ºC). We found no statistically significant changes in film thickness after the welding. A slightly different surface morphology can however be noted, with amorphous carbon deposition present mostly not as a continuous layer, but located in specific regions. When combined with the SEM analysis, these regions may be interpreted as the space between SWCNTs in the film. Since the amorphous carbon is not deposited as a continuous second layer on top of the SWCNTs, a notable increase in thickness is neither seen, nor expected. Thus, we can state that the thickness of the SWCNT films remains the same after the welding under the presented conditions and it is relevant to use thickness of a pristine film for further estimations of specific conductivity and equivalent sheet resistance.

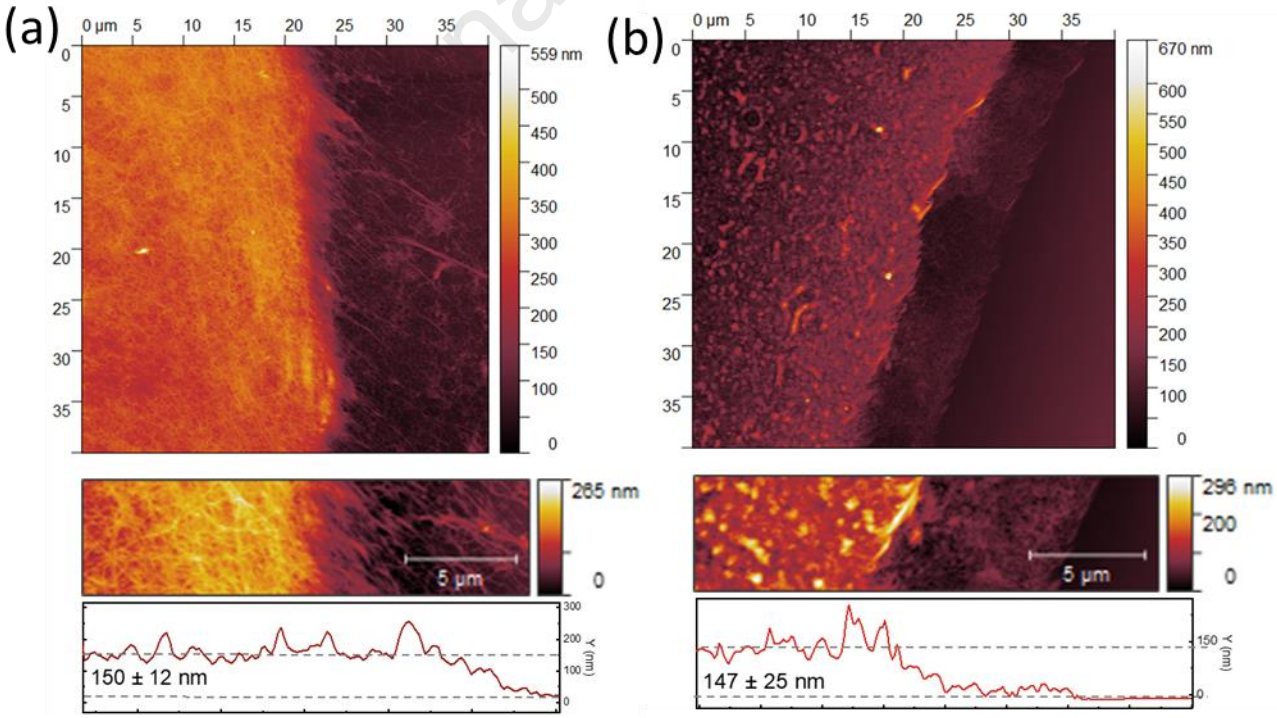

Figure 2. Typical AFM height mapping scans of (a) pristine and (b) welded SWCNT films. The height profiles are shown below each mapping.

We employed UV-vis-NIR spectroscopy to assess the deposition on SWCNT [59]. Though surface decomposition of ethylene was reported to proceed freely at temperatures ~700 ºC [65], here we observe the process to start at higher temperatures: the gradual increase in absorbance started at 1100 ºC (Figure 3a). Moreover, we observed a gradual growth of absorbance assumably due to the ethylene-induced carbon deposits. Similarly, Jiang *et al.* observed the welding to transform the Schottky barriers between metallic and semiconducting nanotubes into near-ohmic junctions [54]. We also note the gradual decrease of equivalent sheet resistance (as well as growth of the electrical conductivity) of the films as well (up to 5 times). It should be stressed that the welding significantly affects (Figure 3b) neither the observed integral defectiveness of the film nor the ensemble of observed radial breathing modes (RBM). This observation coincides with the recent observation of surface pyrolysis of hydrocarbons on nanotubes with the formation of lateral carbon deposits [65–67] proving the formation of similar sp^2 deposits.

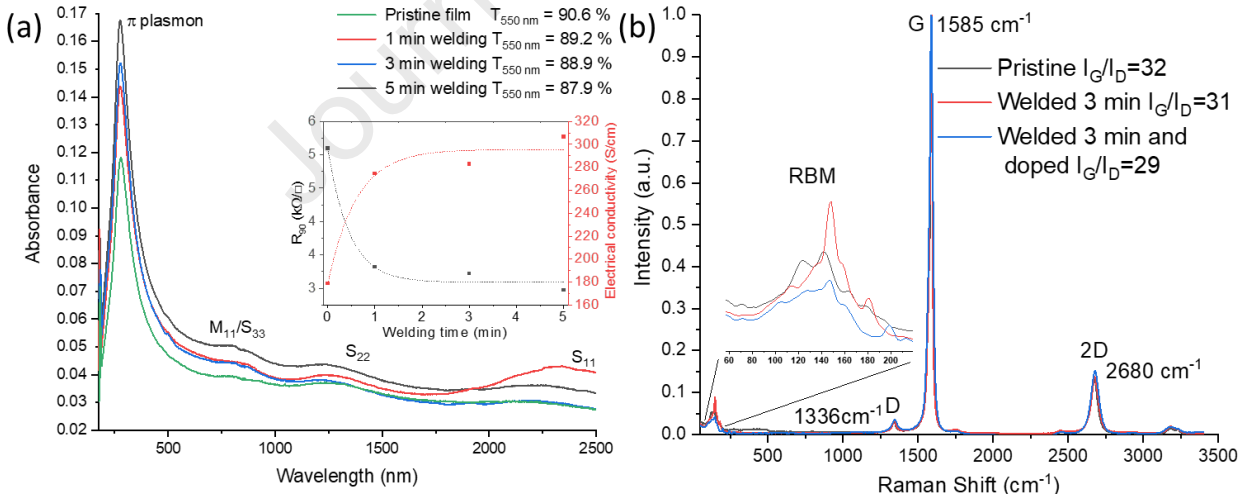

Figure 3. UV-vis-NIR (a) and Raman (b) spectra of pristine and ethylene-treated (1100 ºC) free-standing films; the inset of (a) represents a decrease of the film's equivalent sheet resistance R_{90} and consequently an increase in the electrical conductivity with the treatment, while the inset of (b) represents the enlarged zone of the radial breathing modes (RBM).

To assess the presumed surface deposition of lateral carbon deposits, we performed a TEM observation (Figure 4). We registered no significant changes on the nanotube surface after the short treatment time. The extended deposits formation was minorly observed for both 3 and 5 min (Figures 4b and 4c), while the nanotubes appeared to be coated with lateral carbon deposits during extended treatment times > 10 min (Figure 4d).

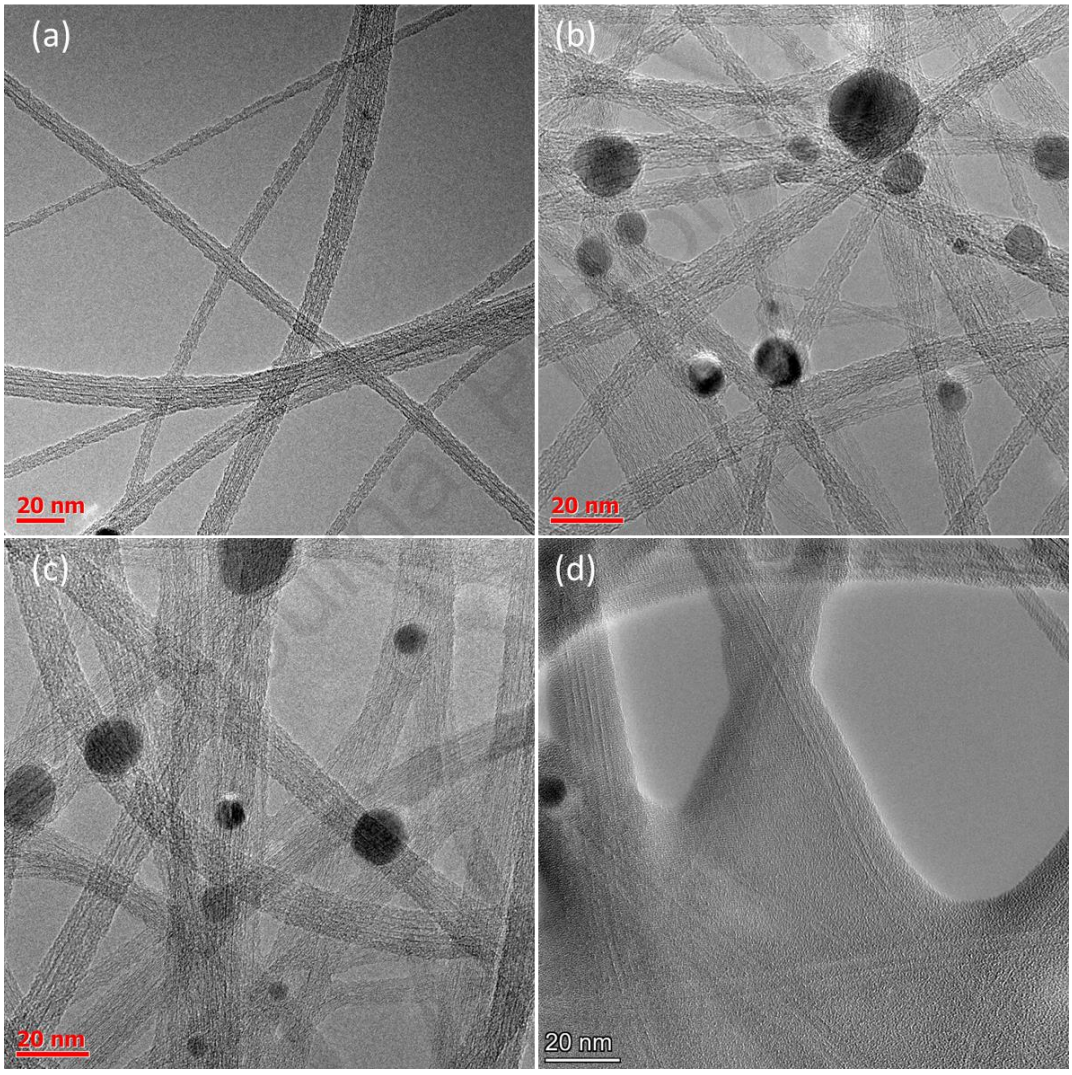

Figure 4. TEM images of SWCNT free-standing films treated with ethylene at 1100°C: (a) pristine free-standing film; (b) 3 min ethylene treatment; (c) 5 min ethylene treatment, showing lateral deposits; (d) 35 min ethylene treatment, showing nanotubes fully coated with deposits.

To assess the welding uniformity, we employed SEM microscopy (Figure 5). The partial formation of deposits occurred after 5 minutes of the treatment (Figure 5b). After 10 minutes, we observed a more uniform coating with apparent thickening of nanotubes (Figure 5c), suggesting that, at the first moments, the junctions are the hottest parts of the SWCNT free-standing film; once the nanotube junctions become fully coated, the deposition proceeds more uniformly reaching even the formation of lamellas (Figure 5d). Additional research is required to establish the relation between the flowrate and temperature on the structure of the carbon deposits.

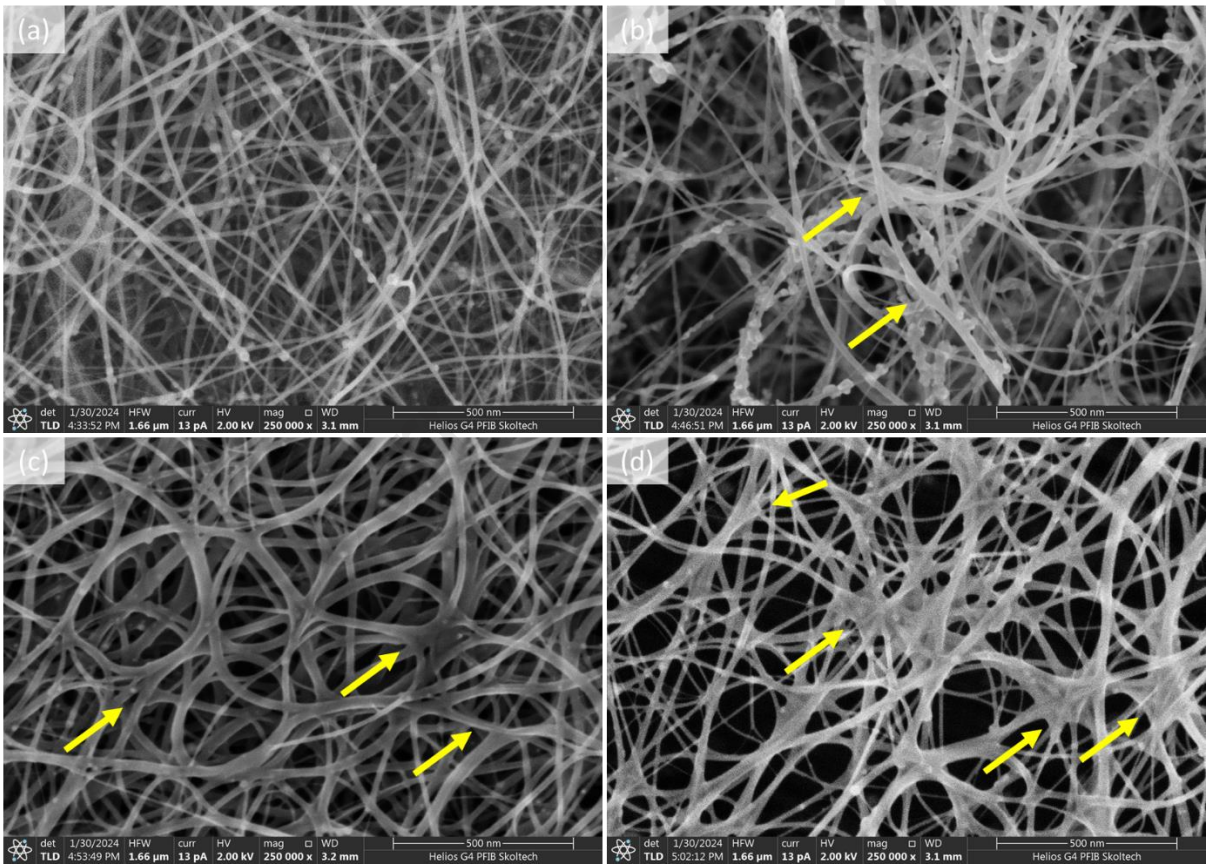

Figure 5. SEM images of different treatment times at 1100°C: (a) pristine free-standing film; (b) 3 min ethylene treatment, showing coating formation and the presence of a closed structure around the bundles; (c) 5 min ethylene treatment showing partial coating of a nanotube bundle; (d) 10 min ethylene treatment showing full coating of SWCNTs. The yellow arrows highlight some of the coating spots.

The temperature dependence of the resistance was performed by a four-probe technique in the region from 100 K to 450 K. The resistance was measured with Keysight 34972A LXI Data Acquisition/Switch Unit (Keysight Technologies, Inc. USA) and the temperature control was provided with Linkam THMS350 Stage chamber under pressure of 0.1 bar with the rate temperature change of 10 °C/min. The results show that after welding the change in TCR after welding resulted in decrease of its values by ~0.1%/K in the range of temperatures under investigation (Figure 6a).

To reveal the change of SWCNT conductivity mechanism after welding, we fitted the experimental data by heterogeneous model [68] (with least-square method):

$$R(T) = R_m \exp\left(-\frac{T_m}{T}\right) + R_t \exp\left(\frac{T_b}{T_s + T}\right),$$

where the first term represents the contribution of nanotubes' intrinsic conductivity and T_m is the least phonons' energy to play role in carriers scattering. The second term describes the tunneling between conducting regions separated by small barriers, and T_s and T_b are parameters of the barrier. R_m and R_t are temperature independent coefficients which depend on geometry of the samples. From approximation we get that the share of the first term in film resistance significantly decreased (Figure 6b). Thus, the impact of tunnelling between conducting regions considerably increased in conductivity mechanism after welding.

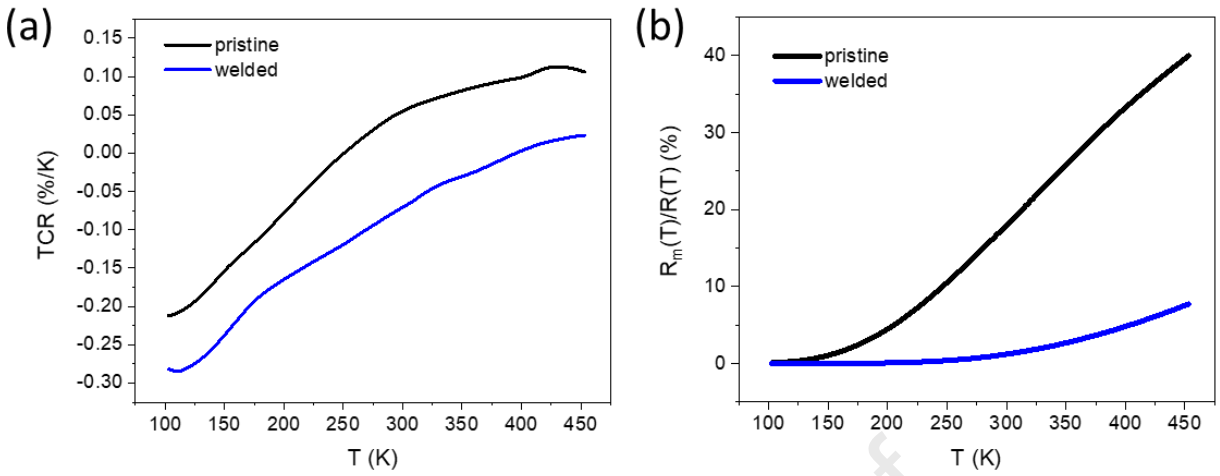

Figure 6. Temperature dependences of TCR (a) and relative contribution of tunnelling between conducting regions (b) for welded (blue) and pristine (black) SWCNT films.

Thus, the ethylene treatment of resistively heated SWCNT free-standing films under low pressure allows nanotube coating with lateral carbon deposits. At the first moments (t<10 min), the coating is non-uniform and presumably appears at the junctions, providing the welding effect: partial doping, decrease of sheet resistance, and non-uniform thickening of junctions observed by SEM. Longer treatment time (>10 min) results in a more uniform coating of the SWCNT surface.

3.2 Influence of welding on mechanical properties of free-standing films

To assess the influence of the welding on the mechanical stability of the SWCNT membranes, we examined the ultimate tensile strength using the procedure reported in [9]. We connected the SWCNT membrane on an aluminium disk with a stepper motor controlled by Nano Arduino (30 μm/s). A needle (Figure 7a; 2 mm in diameter) connected to a pressure sensor penetrates the membrane. We calibrated the device using a known weight.

The ultimate tensile strength (UTS) was derived using the cross-section of the film in the area surrounding the tip of the needle. Pythagorean geometry allowed us to estimate the contact angle change related to the distance, and film thickness was considered to be constant during the measurement until the sample breakage. To determine the measurement accuracy, we used a set of five membranes with a 10% deviation in thickness. At the same time, the values of the tensile strength varied over a wider range (about 25%) due to seemingly inevitable defect formation during the transfer of the films on the holders (Figure S3). Nevertheless, the study of the effect of the modification revealed a more than an order of magnitude growth in the tensile strength (Figure 7b) as well as stiffness, which also indirectly confirms the "welding" of contacts between nanotubes. The last determines the mechanical stability of the entire membrane. The obtained UTS values were proved by classical strain test and similar (with ~12 % variance) to that for membrane penetration studies (Figure 7).

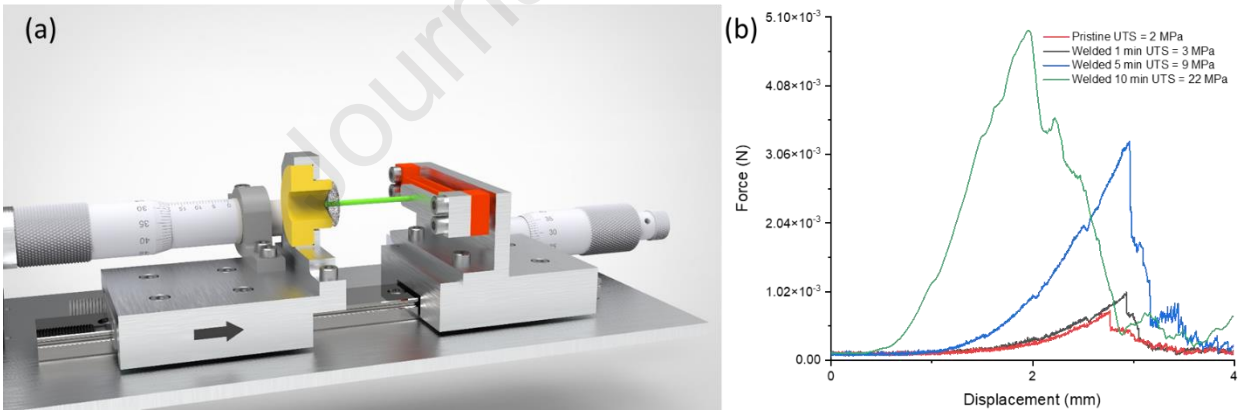

Figure 7. (a) schematic representation of a setup for the ultimate tensile strength (UTS) assessment with a membrane of a holder (yellow), a needle (green), and a pressure sensor (red). (b) force *vs.* displacement measurements of pristine (50% transmittance) and ethylene welded films. The ethylene welding showcased a 66% increase in UTS and a 4% increase in transmittance after 1 min treatment at 1100°C, 1 sccm, P = 0.3 mtorr.

To additionally assess the idea that deposit on the SWCNTs cross-section can increase the strength of the film with coating in comparison with the pristine SWCNTs, molecular dynamics simulation was used. Molecular dynamics (MD) allows one to analyze on an atomic level how the deposit can affect the film strength. To reveal the role of deposits, we combined the experimental observations with non-equilibrium molecular dynamics (MD) simulations using the open-source MD package "large-scale atomic/molecular massively parallel simulator" (LAMMPS) [69,70]. The well-known AIREBO potential is used to reproduce the inter-atomic forces between the carbon atoms; Verlet integration, with a time-step of 1 fs, is employed in particle trajectory calculations. Nosé-Hoover thermostat is used to maintain the temperature at 300 K in all the simulations. As Figure 5 shows numerous nanotube cross-section coating, two structures were considered (Figure 8): (i) two cross-sectioned SWCNTs (15,15) with a length of 20 nm and diameter of 2 nm; and (ii) the same SWCNT with one layer of a graphene deposit around the cross-section.

Periodic boundary conditions along in-plane directions (*x* and *z*) and free boundary conditions along the normal direction (along the *y*-axis) are applied. Figure 8a represents the initial structure of SWCNT (shown in gray color) with one layer of a graphene deposit (shown in light-green color) as an example.

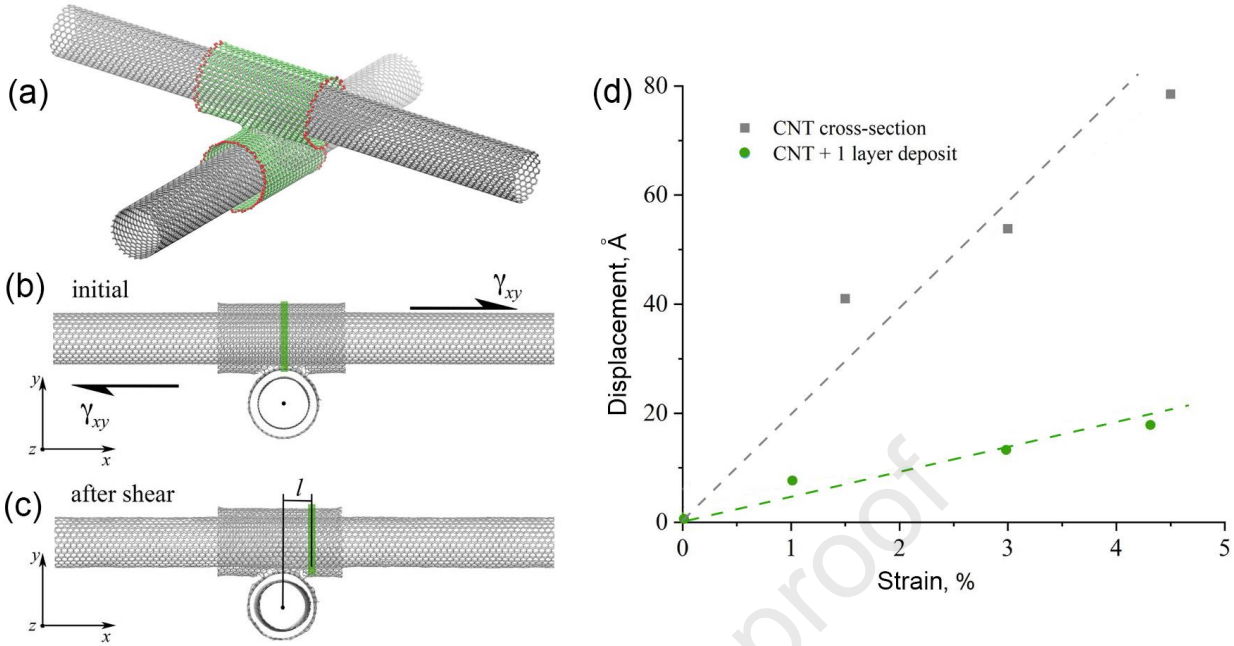

Figure 8. (a) SWCNTs with a layer of graphene deposit after relaxation representing pristine SWCNTs (gray), graphene deposits (green), and CH groups on the edges of graphene flakes (red). Schematic of the SWCNT cross-section with a layer of graphene deposit at the initial state (b) and after shear deformation (c). (d) Displacement of the top SWCNT with respect to the bottom nanotube as the function of shear strain.

At first, relaxation of the system to the equilibrium state is conducted at 300 K. Shear strain is applied to analyze the strengthening effect of the graphene deposit. Figure 8 presents the schematic of the SWCNT cross-section with a layer of the graphene deposit at the initial state (Figure 8b) and after some shear deformation (Figure 8c). The bottom SWCNT is fixed; shear strain is applied to the top SWCNT. The initial position of the top CNT with respect to the bottom SWCNT is marked by green, while the displacement is denoted with l. Displacement of the top SWCNT with respect to the bottom SWCNT was defined during the shear. As can be observed, even one layer of the deposit results in a two-fold decrease in the mutual displacement of the SWCNTs. Thus,

with the MD simulations, we can clearly observe that even a single-layer deposit decreases the value of mutual displacement of the SWCNTs, which further results in the strength increase.

3.3 Influence of welding on equivalent sheet resistance of free-standing films

The decrease in sheet resistance combined with moderate growth of the SWCNT film absorbance opens an opportunity for enhanced performance in transparent conductors. Here, we employ equivalent sheet resistance (the sheet resistance of a film with a 90 % transmittance in the visible region at 550 nm) [59] as (1) a thickness-independent descriptor [57] and (2) one of the key performance indicators for transparent electrode applications [59–61].

Furthermore, the effect can be significantly improved by a doping procedure, which shifts the Fermi level of nanotubes into the valence band, diminishing the Schottky barriers between nanotubes. Remarkably, the Fermi level can be turned in both directions (n- and p- doping) via simple chemical adsorption/coating [71], change of an electrochemical potential [72], or, lastly, via an electrical field [73]. Here, we performed a chemical p-doping with $HAuCl_4$ [71]. Figure 9 illustrates the effect of doping. We observe the suppression of transitions (fingerprint of Fermi level shift) along with significant absorbance growth due to $HAuCl_4$ doping, which also manifests in an additional plasmon peak within the UV region. The optimal doping, thus, is a balance between the increase in conductivity (drops R_{90}) and growth of absorbance (increases R_{90}). Finally, the obtained value of the equivalent sheet resistance (30 Ohm/sq) is among the state-of-the-art for nanotube-based electrodes [59] and among high-performance carbon nanotube conducting elements [74] (electrical conductivity ~ 30,000 S/cm).

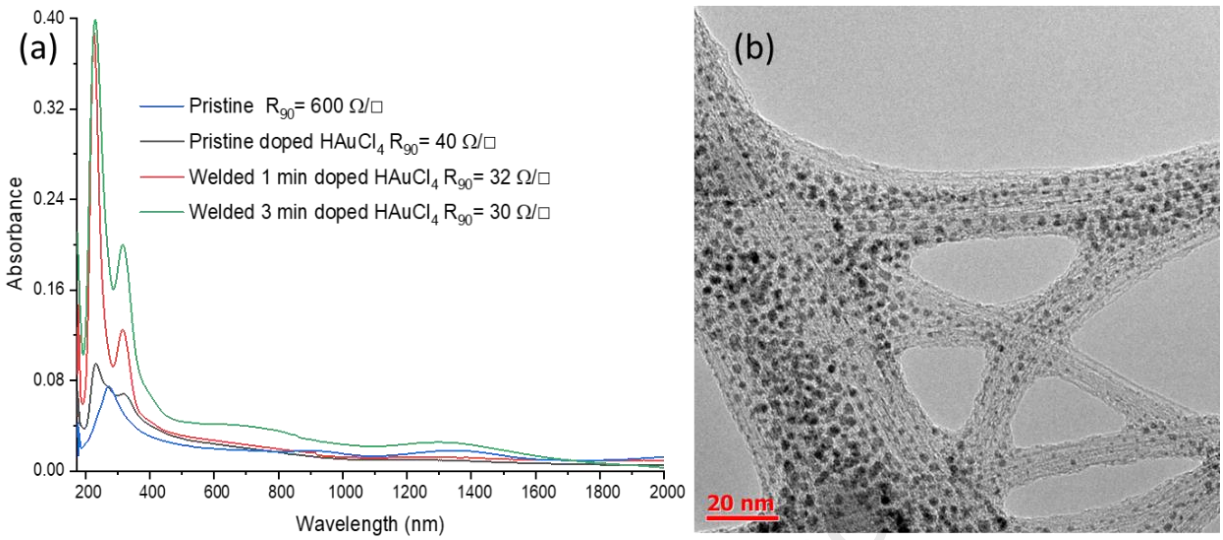

Figure 9. UV-vis-NIR spectra of bilaterally doped samples (a) and HRTEM image of SWCNT welded and doped with $HAuCl_4$ (b).

3.4 Increase in mechanical properties of the free-standing films

Figure 10 provides a typical Ashby material property chart comparison of the ultimate tensile strength of different material classes versus their density. The strength of the pristine and welded free-standing films, when compared to the tensile performance vs. density of other material classes, is high. The strength of the welded SWCNT films is in the same order of magnitude as polymers and other high-performance membrane materials but at 2-3 orders of magnitude lower in density. It should be noted that for micrometer scale materials, the SWCNT free-standing films here have ultimate tensile strength values one order of magnitude smaller than high-performance ceramics, composites, and metals.

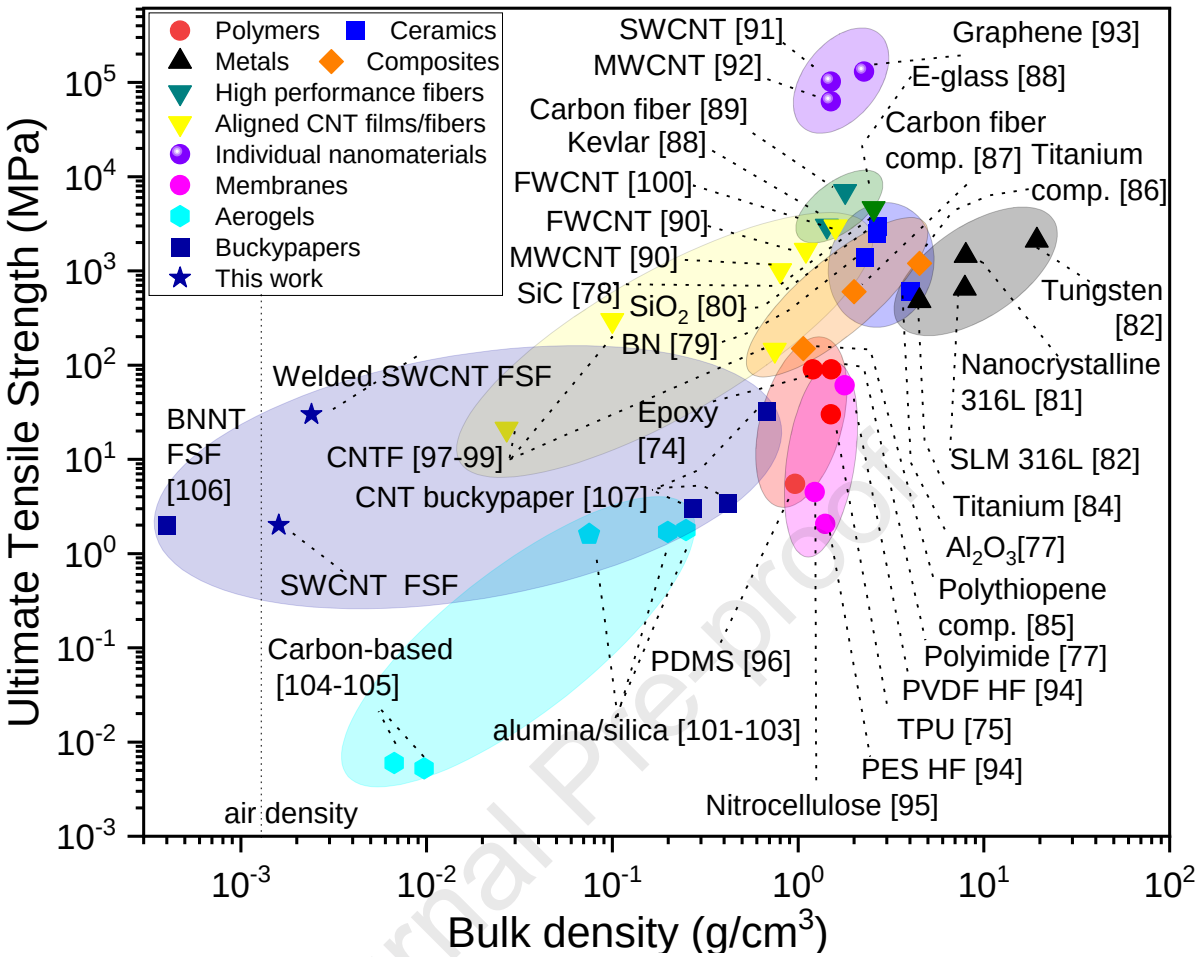

Figure 10. Ashby chart for the tensile performance of different material classes.[74–107]

Surprisingly, the welded films are only 1-2 orders of magnitude lower than aligned CNT films in terms of strength. Aligned films are known to have exceptionally high mechanical properties when tested parallel to the alignment direction [100] In the case of randomly oriented films, this relatively small difference is surprising since there is no perfect alignment of the SWCNTs with the applied testing force. Recently, carbon nanotube resistive heating was shown to promote crystallization/phase transition of inorganic matrices within the joint composites providing additional opportunities for the welded films [108].

4. CONCLUSIONS

We report the new approach for the modification of junctions between carbon nanotubes by means of a chemical reaction (namely, ethylene pyrolysis) on the surface of resistively heated free-standing films. The pyrolysis results in the lateral carbon deposits concentrating at first on the junctions (as the most resistive and, thereby, the hottest points of the free-standing film) and then on all the nanotubes. We observe that welding has a complex effect on the free-standing film: partial doping, decreased sheet resistance, and non-uniform thickening of junctions. The welding also alters characteristics of SWCNT films, such as the equivalent sheet resistance and ultimate tensile strength (reaches 22 MPa). The MD simulations show the latter happens due to an inhibited sliding effect between two carbon nanotubes at the welded junction. The obtained value of the equivalent sheet resistance for welded SWCNT free-standing films after doping with $HAuCl_4$ (30 Ohm/sq; electrical conductivity ~ 30,000 S/cm) is among the state-of-the-art nanotube-based electrodes. Thus, the method allows the SWCNT junction engineering via chemical reactions induced by resistive heating of a free-standing (or some other assembly like yearn, fiber, pattern, aerogel, *etc.*). The proposed technique might find use for filters and protective membranes due to enhanced mechanical properties as well as transparent electrodes for touchscreens and solar cells along with aerosol filters and biomedical scaffolds after the modification of optoelectronic properties.

CRediT authorship contribution statement

Javier A. Ramirez B.: Methodology, Software, Validation, Investigation., Data curation, Writing—original draft preparation. **Dmitry V. Krasnikov:** Conceptualization, Validation, Resources, Writing —review and editing, Funding acquisition, Supervision. **Hassaan A. Butt:** Methodology, Software, Validation, Writing —review and editing. **Veronika A. Dmitrieva:** Formal analysis, Investigation. **Oleg R. Trepalin:** Formal analysis, Investigation. **Aliya R. Vildanova:** Investigation, Data curation Writing —review and editing. **Vladislav A. Kondrashov:** Methodology, Software. **Anastasia E. Goldt:** Formal analysis, Investigation, Data curation. **Dmitry V. Dzhurinskiy:** Formal analysis, Investigation, Software. **Julia A. Baimova:** Software, Formal analysis, Investigation, Writing —review and editing. **Rajath Alexander:** Formal analysis, Validation. **Amit Kushal**: Formal analysis, Validation. **Kinshuk Dasgupta:** Validation, Writing —review and editing. **Omid Akhavan:** Formal analysis, Investigation, Data curation. **Albert G. Nasibulin:** Conceptualization, Resources, Writing—review and editing, Funding acquisition, Project administration.

Notes

The authors declare no competing financial interests.

ACKNOWLEDGMENTS

The authors acknowledge Dr. Stepan Romanov for the partial design of the setup. A.G.N. acknowledges the support by the Russian Science Foundation (No. 21-72-20050: aerosol CVD synthesis, welding and characterization of carbon nanotubes). MD simulation was conducted by J.B. and supported by the State Assignment of IMSP RAS (Young Scientist Laboratory).

REFERENCES

[1] S. Rathinavel, K. Priyadharshini, D. Panda, A review on carbon nanotube: An overview of synthesis, properties, functionalization, characterization, and the application, Materials Science and Engineering: B 268 (2021) 115095. https://doi.org/10.1016/j.mseb.2021.115095.

[2] M.S. Dresselhaus, G. Dresselhaus, J.C. Charlier, E. Hernandez, Electronic, thermal and mechanical properties of carbon nanotubes, Philosophical Transactions of the Royal Society of London Series A-Mathematical Physical and Engineering Sciences 362 (2004) 2065–2098. https://doi.org/10.1098/rsta.2004.1430.

[3] S. Bellucci, Carbon nanotubes: physics and applications, Physica Status Solidi (c) 2 (2005) 34–47. https://doi.org/10.1002/pssc.200460105.

[4] A. Hirsch, C. Backes, Carbon Nanotube Science. Synthesis, Properties and Applications. By Peter J. F. Harris., Cambridge Unversity press, 2010. https://doi.org/10.1002/anie.201000314.

[5] M. Meyyappan, Carbon Nanotubes, CRC Press, 2004. https://doi.org/10.1201/9780203494936.

[6] M.F.L. De Volder, S.H. Tawfick, R.H. Baughman, A.J. Hart, Carbon Nanotubes: Present and Future Commercial Applications, Science (1979) 339 (2013) 535–539. https://doi.org/10.1126/science.1222453.

[7] A. Kausar, H. Ilyas, M. Siddiq, Current Research Status and Application of Polymer/Carbon Nanofiller Buckypaper: A Review, Polymer - Plastics Technology and Engineering 56 (2017) 1780–1800. https://doi.org/10.1080/03602559.2017.1289407.

[8] Md.H.-O. Rashid, S.F. Ralph, Carbon Nanotube Membranes: Synthesis, Properties, and Future Filtration Applications, Nanomaterials 7 (2017) 99. https://doi.org/10.3390/nano7050099.

[9] A.G. Nasibulin, A. Kaskela, K. Mustonen, A.S. Anisimov, V. Ruiz, S. Kivistö, S. Rackauskas, M.Y. Timmermans, M. Pudas, B. Aitchison, M. Kauppinen, D.P. Brown, O.G. Okhotnikov, E.I. Kauppinen, Multifunctional free-standing single-walled carbon nanotube films, ACS Nano 5 (2011) 3214–3221. https://doi.org/10.1021/nn200338r.

[10] D. Janas, M. Rdest, K.K.K. Koziol, Free-standing films from chirality-controlled carbon nanotubes, Mater Des 121 (2017) 119–125. https://doi.org/10.1016/j.matdes.2017.02.062.

[11] P. Hou, F. Zhang, L. Zhang, C. Liu, H. Cheng, Synthesis of Carbon Nanotubes by Floating Catalyst Chemical Vapor Deposition and Their Applications, Adv Funct Mater 2108541 (2021) 2108541. https://doi.org/10.1002/adfm.202108541.

[12] A. Tcharkhtchi, N. Abbasnezhad, M. Zarbini Seydani, N. Zirak, S. Farzaneh, M. Shirinbayan, An overview of filtration efficiency through the masks: Mechanisms of the

aerosols penetration, Bioact Mater 6 (2021) 106–122. https://doi.org/10.1016/j.bioactmat.2020.08.002.

[13] V. Gubarev, M. Krivokorytov, V. Krivtsun, N. Novikova, S. Yakunin, A. Pal, J.A. Ramirez B, D. Krasnikov, V. Medvedev, A.G. Nasibulin, Ar permeability through densified single-walled carbon nanotube-based membranes, J Appl Phys 133 (2023). https://doi.org/10.1063/5.0135082.

[14] T. Guan, M. Yao, Use of carbon nanotube filter in removing bioaerosols, J Aerosol Sci 41 (2010) 611–620. https://doi.org/10.1016/j.jaerosci.2010.03.002.

[15] V.M. Gubarev, V.Y. Yakovlev, M.G. Sertsu, O.F. Yakushev, V.M. Krivtsun, Y.G. Gladush, I.A. Ostanin, A. Sokolov, F. Schäfers, V. V. Medvedev, A.G. Nasibulin, Single-walled carbon nanotube membranes for optical applications in the extreme ultraviolet range, Carbon 155 (2019) 734–739. https://doi.org/10.1016/j.carbon.2019.09.006.

[16] F. Muench, L. Sun, T. Kottakkat, M. Antoni, S. Schaefer, U. Kunz, L. Molina-Luna, M. Duerrschnabel, H.J. Kleebe, S. Ayata, C. Roth, W. Ensinger, Free-standing networks of core-shell metal and metal oxide nanotubes for glucose sensing, ACS Appl Mater Interfaces 9 (2017) 771–781. https://doi.org/10.1021/acsami.6b13979.

[17] S. Chun, W. Son, C. Choi, Flexible pressure sensors using highly-oriented and free-standing carbon nanotube sheets, Carbon 139 (2018) 586–592. https://doi.org/10.1016/j.carbon.2018.07.005.

[18] E.X. Ding, A. Hussain, S. Ahmad, Q. Zhang, Y. Liao, H. Jiang, E.I. Kauppinen, High-performance transparent conducting films of long single-walled carbon nanotubes synthesized from toluene alone, Nano Res 13 (2020) 112–120. https://doi.org/10.1007/s12274-019-2581-7.

[19] L. Yu, C. Shearer, J. Shapter, Recent Development of Carbon Nanotube Transparent Conductive Films, Chem Rev 116 (2016) 13413–13453. https://doi.org/10.1021/acs.chemrev.6b00179.

[20] S. Horike, Y. Kuwahara, Q. Wei, K. Kirihara, M. Mukaida, T. Saito, Large thermoelectric power factor in wafer-scale free-standing single-walled carbon nanotube films, Appl Phys Lett 118 (2021) 173902. https://doi.org/10.1063/5.0047089.

[21] J. Khongthong, N.I. Raginov, E.M. Khabushev, A.E. Goldt, V.A. Kondrashov, D.M. Russakov, S.D. Shandakov, D. V. Krasnikov, A.G. Nasibulin, Aerosol doping of SWCNT films with p- and n-type dopants for optimizing thermoelectric performance, Carbon 218 (2024). https://doi.org/10.1016/j.carbon.2023.118670.

[22] B. Pandit, S.R. Dhakate, B.P. Singh, B.R. Sankapal, Free-standing flexible MWCNTs bucky paper: Extremely stable and energy efficient supercapacitive electrode, Electrochim Acta 249 (2017) 395–403. https://doi.org/10.1016/j.electacta.2017.08.013.

[23] L.F. Cui, L. Hu, J.W. Choi, Y. Cui, Light-weight free-standing carbon nanotube-silicon films for anodes of lithium ion batteries, ACS Nano 4 (2010) 3671–3678. https://doi.org/10.1021/nn100619m.

[24] Y. Hu, D. Ye, B. Luo, H. Hu, X. Zhu, S. Wang, L. Li, S. Peng, L. Wang, A Binder-Free and Free-Standing Cobalt Sulfide@Carbon Nanotube Cathode Material for Aluminum-Ion Batteries, Advanced Materials 30 (2018). https://doi.org/10.1002/adma.201703824.

[25] H. Wang, J. Jia, P. Song, Q. Wang, D. Li, S. Min, C. Qian, L. Wang, Y.F. Li, C. Ma, T. Wu, J. Yuan, M. Antonietti, G.A. Ozin, Efficient Electrocatalytic Reduction of CO2 by Nitrogen-Doped Nanoporous Carbon/Carbon Nanotube Membranes: A Step Towards the Electrochemical CO2 Refinery, Angewandte Chemie - International Edition 56 (2017) 7847–7852. https://doi.org/10.1002/anie.201703720.

[26] R. Dong, M. Pfeffermann, H. Liang, Z. Zheng, X. Zhu, J. Zhang, X. Feng, Large-Area, Free-Standing, Two-Dimensional Supramolecular Polymer Single-Layer Sheets for Highly Efficient Electrocatalytic Hydrogen Evolution, Angewandte Chemie 127 (2015) 12226–12231. https://doi.org/10.1002/ange.201506048.

[27] S.A. Romanov, A.E. Aliev, B. V. Fine, A.S. Anisimov, A.G. Nasibulin, Highly efficient thermophones based on freestanding single-walled carbon nanotube films, Nanoscale Horiz (2019) 1158–1163. https://doi.org/10.1039/c9nh00164f.

[28] M. Rabbani, A.W. Syed, S. Khalid, M.A. Mohammad, Fabrication and characterization of a thermophone based on laser-scribed graphene intercalated with multiwalled carbon nanotubes, Nanomaterials 11 (2021). https://doi.org/10.3390/nano11112874.

[29] T.N. Kurtukova, D.S. Kopylova, N.I. Raginov, E.M. Khabushev, I. V. Novikov, S.I. Serebrennikova, D. V. Krasnikov, A.G. Nasibulin, Plasma-treated carbon nanotubes for fast infrared bolometers, Appl Phys Lett 122 (2023). https://doi.org/10.1063/5.0140030.

[30] D.S. Kopylova, F.S. Fedorov, A.A. Alekseeva, E.P. Gilshteyn, A.P. Tsapenko, A. V Bubis, A.K. Grebenko, Z.I. Popov, P.B. Sorokin, Y.G. Gladush, A.S. Anisimov, A.G. Nasibulin, Holey single-walled carbon nanotubes for ultra-fast broadband bolometers †, Nanoscale 10 (2018) 18665. https://doi.org/10.1039/c8nr05925j.

[31] X. Kang, C. Li, W. Cui, H. Yuan, Z. Wang, Z. Zheng, X. Cui, Facile electro-thermal igniters based on freestanding CNTs films for ignition of energetic materials, J Phys D Appl Phys (2022). https://doi.org/10.1088/1361-6463/ac9486.

[32] M.Y. Koo, G.W. Lee, The Joule Heating Effect of a Foldable and Cuttable Sheet Made of SWCNT/ANF Composite, Nanomaterials 12 (2022). https://doi.org/10.3390/nano12162780.

[33] J.A. Ramirez B., D. V. Krasnikov, V. V. Gubarev, I. V. Novikov, V.A. Kondrashov, A. V. Starkov, M.S. Krivokorytov, V. V. Medvedev, Y.G. Gladush, A.G. Nasibulin, Renewable single-walled carbon nanotube membranes for extreme ultraviolet pellicle applications, Carbon 198 (2022) 364–370. https://doi.org/10.1016/j.carbon.2022.07.014.

[34] G. Zainab, N. Iqbal, A.A. Babar, C. Huang, X. Wang, J. Yu, B. Ding, Free-standing, spider-web-like polyamide/carbon nanotube composite nanofibrous membrane impregnated with polyethyleneimine for CO2 capture, Composites Communications 6 (2017) 41–47. https://doi.org/10.1016/j.coco.2017.09.001.

[35] D. Suzuki, Y. Ochiai, Y. Nakagawa, Y. Kuwahara, T. Saito, Y. Kawano, Fermi-level-controlled semiconducting-separated carbon nanotube films for flexible terahertz imagers, ACS Appl Nano Mater 1 (2018) 2469–2475. https://doi.org/10.1021/acsanm.8b00421.

[36] M.G. Burdanova, G.M. Katyba, R. Kashtiban, G.A. Komandin, E. Butler-Caddle, M. Staniforth, A.A. Mkrtchyan, D. V. Krasnikov, Y.G. Gladush, J. Sloan, A.G. Nasibulin, J. Lloyd-Hughes, Ultrafast, high modulation depth terahertz modulators based on carbon nanotube thin films, Carbon 173 (2021) 245–252. https://doi.org/10.1016/j.carbon.2020.11.008.

[37] I. V. Novikov, N.I. Raginov, D. V. Krasnikov, S.S. Zhukov, K. V. Zhivetev, A. V. Terentiev, D.A. Ilatovskii, A. Elakshar, E.M. Khabushev, A.K. Grebenko, S.A. Kuznetsov, S.D. Shandakov, B.P. Gorshunov, A.G. Nasibulin, Fast liquid-free patterning of SWCNT films for electronic and optical applications, Chemical Engineering Journal (2024) 149733. https://doi.org/10.1016/j.cej.2024.149733.

[38] J.H. Zhang, Y.Y. Zhang, Membrane nanotubes: Novel communication between distant cells, Sci China Life Sci 56 (2013) 994–999. https://doi.org/10.1007/s11427-013-4548-3.

[39] A. Chauveau, A. Aucher, P. Eissmann, E. Vivier, D.M. Davis, Membrane nanotubes facilitate long-distance interactions between natural killer cells and target cells, Proc Natl Acad Sci U S A 107 (2010) 5545–5550. https://doi.org/10.1073/pnas.0910074107.

[40] J.R. Sanchez-Valencia, T. Dienel, O. Gröning, I. Shorubalko, A. Mueller, M. Jansen, K. Amsharov, P. Ruffieux, R. Fasel, Controlled synthesis of single-chirality carbon nanotubes, Nature 512 (2014) 61–64. https://doi.org/10.1038/nature13607.

[41] P.-C. Ma, N.A. Siddiqui, G. Marom, J.-K. Kim, Dispersion and functionalization of carbon nanotubes for polymer-based nanocomposites: A review, 41 (2010) 1345–1367. https://doi.org/10.1016/j.compositesa.2010.07.003.

[42] M.S.P. Shaffer, S.A. Hodge, M.K. Bayazit, K.S. Coleman, M.S.P. Shaffer, Unweaving the rainbow: a review of the relationship between single-walled carbon nanotube molecular structures and their chemical reactivity, Chem Soc Rev 41 (2012) 4409. https://doi.org/10.1039/c2cs15334c.

[43] F. Hof, S. Bosch, S. Eigler, F. Hauke, A. Hirsch, New basic insight into reductive functionalization sequences of single walled carbon nanotubes (SWCNTs), J Am Chem Soc 135 (2013) 18385–18395. https://doi.org/10.1021/ja4063713.

[44] M. Schirowski, G. Abellán, E. Nuin, J. Pampel, C. Dolle, V. Wedler, T.P. Fellinger, E. Spiecker, F. Hauke, A. Hirsch, Fundamental Insights into the Reductive Covalent Cross-Linking of Single-Walled Carbon Nanotubes, J Am Chem Soc 140 (2018) 3352–3360. https://doi.org/10.1021/jacs.7b12910.

[45] E.M. Khabushev, D.V. Krasnikov, J.V. Kolodiazhnaia, A.V. Bubis, A.G. Nasibulin, Structure-dependent performance of single-walled carbon nanotube films in transparent and conductive applications, Carbon 161 (2020). https://doi.org/10.1016/j.carbon.2020.01.068.

[46] A.A. Tonkikh, V.A. Eremina, E.A. Obraztsova, D.A. Musatov, A.Y. Pereyaslavtsev, E.I. Kauppinen, E.D. Obraztsova, Tunable Doping and Characterization of Single-Wall Carbon Nanotube Macrosystems for Electrode Material Applications, ACS Appl Nano Mater (2021) acsanm.1c00411. https://doi.org/10.1021/acsanm.1c00411.

[47] S. Bhusal, S. Sihn, V. Varshney, A.K. Roy, A study on mechanical strength and stability of partially-fused carbon nanotube junctions, Carbon Trends 3 (2021) 39. https://doi.org/10.1016/j.cartre.2021.10.

[48] S. Ozden, G. Brunetto, N.S. Karthiselva, D.S. Galvão, A. Roy, S.R. Bakshi, C.S. Tiwary, P.M. Ajayan, Controlled 3D Carbon Nanotube Structures by Plasma Welding, Adv Mater Interfaces 3 (2016). https://doi.org/10.1002/admi.201500755.

[49] A.Y. Gerasimenko, A. V. Kuksin, Y.P. Shaman, E.P. Kitsyuk, Y.O. Fedorova, D.T. Murashko, A.A. Shamanaev, E.M. Eganova, A. V. Sysa, M.S. Savelyev, D. V. Telyshev, A.A. Pavlov, O.E. Glukhova, Hybrid Carbon Nanotubes–Graphene Nanostructures: Modeling, Formation, Characterization, Nanomaterials 12 (2022). https://doi.org/10.3390/nano12162812.

[50] a V Krasheninnikov, F. Banhart, Engineering of nanostructured carbon materials with electron or ion beams., Nat Mater 6 (2007) 723–733. https://doi.org/10.1038/nmat1996.

[51] K. Mustonen, A.G. Nasibulin, M. Pudas, M. Kauppinen, H. Jiang, K. Grigoras, J. Raula, E.I. Kauppinen, Reinforcing randomly oriented transparent freestanding single-walled carbon nanotube films, Carbon 62 (2013). https://doi.org/10.1016/j.carbon.2013.05.072.

[52] S. Ahmad, K. Mustonen, B. McLean, H. Jiang, Q. Zhang, A. Hussain, A.T. Khan, E.X. Ding, Y. Liao, N. Wei, M.R.A. Monazam, A.G. Nasibulin, J. Kotakoski, A.J. Page, E.I. Kauppinen, Hybrid Low-Dimensional Carbon Allotropes Formed in Gas Phase, Adv Funct Mater 30 (2020). https://doi.org/10.1002/adfm.202005016.

[53] S. Zhang, A. Hao, N. Nguyen, A. Oluwalowo, Z. Liu, Y. Dessureault, J.G. Park, R. Liang, Carbon nanotube/carbon composite fiber with improved strength and electrical conductivity via interface engineering, Carbon 144 (2019) 628–638. https://doi.org/10.1016/j.carbon.2018.12.091.

[54] S. Jiang, P.-X. Hou, M.-L. Chen, B.-W. Wang, D.-M. Sun, D.-M. Tang, Q. Jin, Q.-X. Guo, D.-D. Zhang, J.-H. Du, K.-P. Tai, J. Tan, E.I. Kauppinen, C. Liu, H.-M. Cheng, Ultrahigh-performance transparent conductive films of carbon-welded isolated single-wall carbon nanotubes, Sci Adv 4 (2018). https://doi.org/10.1126/sciadv.aap9264.

[55] H.W. Ch Postma, M. de Jonge, Z. Yao, C. Dekker, Electrical transport through carbon nanotube junctions created by mechanical manipulation, 2000.

[56] S.A. Romanov, A.A. Alekseeva, E.M. Khabushev, D. V. Krasnikov, A.G. Nasibulin, Rapid, efficient, and non-destructive purification of single-walled carbon nanotube films from metallic impurities by Joule heating, Carbon 168 (2020) 193–200. https://doi.org/10.1016/j.carbon.2020.06.068.

[57] A. Kaskela, A.G. Nasibulin, M.Y. Timmermans, B. Aitchison, A. Papadimitratos, Y. Tian, Z. Zhu, H. Jiang, D.P. Brown, A. Zakhidov, E.I. Kauppinen, Aerosol-Synthesized SWCNT Networks with Tunable Conductivity and Transparency by a Dry Transfer Technique, Nano Lett 10 (2010) 4349–4355. https://doi.org/10.1021/nl101680s.

[58] G.A. Ermolaev, A.P. Tsapenko, V.S. Volkov, A.S. Anisimov, Y.G. Gladush, A.G. Nasibulin, Express determination of thickness and dielectric function of single-walled carbon nanotube films, Appl Phys Lett 116 (2020) 231103. https://doi.org/10.1063/5.0012933.

[59] D.A. Ilatovskii, E.P. Gilshtein, O.E. Glukhova, A.G. Nasibulin, Transparent Conducting Films Based on Carbon Nanotubes: Rational Design toward the Theoretical Limit, Advanced Science 9 (2022) 2201673. https://doi.org/10.1002/ADVS.202201673.

[60] Q. Zhang, N. Wei, P. Laiho, E.I. Kauppinen, Recent Developments in Single-Walled Carbon Nanotube Thin Films Fabricated by Dry Floating Catalyst Chemical Vapor Deposition, Top Curr Chem 375 (2017) 90. https://doi.org/10.1007/s41061-017-0178-8.

[61] I. V. Novikov, D. V. Krasnikov, I.H. Lee, E.E. Agafonova, S.I. Serebrennikova, Y. Lee, S. Kim, J. Nam, V.A. Kondrashov, J. Han, I.I. Rakov, A.G. Nasibulin, I. Jeon, Aerosol CVD Carbon Nanotube Thin Films: From Synthesis to Advanced Applications: A Comprehensive Review, Advanced Materials (2025). https://doi.org/10.1002/adma.202413777.

[62] A.E. Goldt, O.T. Zaremba, M.O. Bulavskiy, F.S. Fedorov, K. V. Larionov, A.P. Tsapenko, Z.I. Popov, P. Sorokin, A.S. Anisimov, H. Inani, J. Kotakoski, K. Mustonen, A.G. Nasibulin, Correction: Highly efficient bilateral doping of single-walled carbon nanotubes, J Mater Chem C Mater 9 (2021). https://doi.org/10.1039/d1tc90195h.

[63] A.G. Nasibulin, A. Moisala, D.P. Brown, H. Jiang, E.I. Kauppinen, A novel aerosol method for single walled carbon nanotube synthesis, Chem Phys Lett 402 (2005) 227–232. https://doi.org/10.1016/j.cplett.2004.12.040.

[64] I. V. Novikov, E.M. Khabushev, D. V. Krasnikov, A. V. Bubis, A.E. Goldt, S.D. Shandakov, A.G. Nasibulin, Residence time effect on single-walled carbon nanotube synthesis in an aerosol CVD reactor, Chemical Engineering Journal 420 (2021) 129869. https://doi.org/10.1016/j.cej.2021.129869.

[65] D.V. Krasnikov, V.L. Kuznetsov, A.I. Romanenko, A.N. Shmakov, Side reaction in catalytic CVD growth of carbon nanotubes: Surface pyrolysis of a hydrocarbon precursor with the formation of lateral carbon deposits, Carbon 139 (2018). https://doi.org/10.1016/j.carbon.2018.06.033.

[66] H. Allouche, M. Monthioux, Chemical vapor deposition of pyrolytic carbon on carbon nanotubes. Part 2. Texture and structure, Carbon 43 (2005) 1265–1278. https://doi.org/10.1016/j.carbon.2004.12.023.

[67] M. Monthioux, H. Allouche, R.L. Jacobsen, Chemical vapour deposition of pyrolytic carbon on carbon nanotubes, Carbon 44 (2006) 3183–3194. https://doi.org/10.1016/j.carbon.2006.07.001.

[68] A.B. Kaiser, G. Düsberg, S. Roth, Heterogeneous model for conduction in carbon nanotubes, Phys Rev B 57 (1998) 1418–1421. https://doi.org/10.1103/PhysRevB.57.1418.

[69] A.P. Thompson, H.M. Aktulga, R. Berger, D.S. Bolintineanu, W.M. Brown, P.S. Crozier, P.J. in 't Veld, A. Kohlmeyer, S.G. Moore, T.D. Nguyen, R. Shan, M.J. Stevens, J. Tranchida, C. Trott, S.J. Plimpton, LAMMPS - a flexible simulation tool for particle-based materials modeling at the atomic, meso, and continuum scales, Comput Phys Commun 271 (2022). https://doi.org/10.1016/j.cpc.2021.108171.

[70] S. Plimpton, Fast parallel algorithms for short-range molecular dynamics, J Comput Phys 117 (1995). https://doi.org/10.1006/jcph.1995.1039.

[71] A.P. Tsapenko, S.A. Romanov, D.A. Satco, D. V. Krasnikov, P.M. Rajanna, M. Danilson, O. Volobujeva, A.S. Anisimov, A.E. Goldt, A.G. Nasibulin, Aerosol-Assisted Fine-Tuning of Optoelectrical Properties of SWCNT Films, Journal of Physical Chemistry Letters 10 (2019) 3961–3965. https://doi.org/10.1021/acs.jpclett.9b01498.

[72] D.S. Kopylova, D.A. Satco, E.M. Khabushev, A. V. Bubis, D. V. Krasnikov, T. Kallio, A.G. Nasibulin, Electrochemical enhancement of optoelectronic performance of transparent and conducting single-walled carbon nanotube films, Carbon 167 (2020) 244–248. https://doi.org/10.1016/j.carbon.2020.05.103.

[73] J. Zou, Q. Zhang, Advances and Frontiers in Single-Walled Carbon Nanotube Electronics, Advanced Science 8 (2021). https://doi.org/10.1002/advs.202102860.

[74] M.R. Chetyrkina, H.A. Butt, M.O. Bulavskiy, M.A. Zhilyaeva, D. V. Krasnikov, F.S. Fedorov, B. Mikladal, S.D. Shandakov, A.G. Nasibulin, Approaching Technological Limit for Wet-Pulling Technique, Adv Eng Mater 26 (2024). https://doi.org/10.1002/adem.202301592.

[75] L. Li, Z. Cai, Flame-retardant performance of transparent and tensile-strength-enhanced epoxy resins, Polymers (Basel) 12 (2020). https://doi.org/10.3390/polym12020317.

[76] I. V. Novikov, D. V. Krasnikov, A.M. Vorobei, Y.I. Zuev, H.A. Butt, F.S. Fedorov, S.A. Gusev, A.A. Safonov, E. V. Shulga, S.D. Konev, I. V. Sergeichev, S.S. Zhukov, T. Kallio, B.P. Gorshunov, O.O. Parenago, A.G. Nasibulin, Multifunctional Elastic Nanocomposites with Extremely Low Concentrations of Single-Walled Carbon Nanotubes, ACS Appl Mater Interfaces 14 (2022) 18866–18876. https://doi.org/10.1021/acsami.2c01086.

[77] T. Agag, T. Koga, T. Takeichi, Studies on thermal and mechanical properties of polyimide-clay nanocomposites, Polymer (Guildf) 42 (2001). https://doi.org/10.1016/S0032-3861(00)00824-7.

[78] B.D. Flinn, R.K. Bordia, A. Zimmermann, J. Rödel, Evolution of defect size and strength of porous alumina during sintering, J Eur Ceram Soc 20 (2000). https://doi.org/10.1016/S0955-2219(00)00133-3.

[79] S. Cao, J. Wang, H. Wang, Effect of heat treatment on the microstructure and tensile strength of KD-II SiC fibers, Materials Science and Engineering: A 673 (2016). https://doi.org/10.1016/j.msea.2016.07.066.

[80] Z. Cheng, H. Yu, L. Li, Y. Li, X. Zhang, H. Jiang, Preparation of the boron nitride fibers by chemical reaction, in: Adv Mat Res, 2009. https://doi.org/10.4028/www.scientific.net/AMR.66.191.

[81] C.E. Athanasiou, Y. Bellouard, A monolithic micro-tensile tester for investigating silicon dioxide polymorph micromechanics, fabricated and operated using a femtosecond laser, Micromachines (Basel) 6 (2015). https://doi.org/10.3390/mi6091365.

[82] X.H. Chen, J. Lu, L. Lu, K. Lu, Tensile properties of a nanocrystalline 316L austenitic stainless steel, Scr Mater 52 (2005). https://doi.org/10.1016/j.scriptamat.2005.01.023.

[83] C. Qiu, M. Al Kindi, A.S. Aladawi, I. Al Hatmi, A comprehensive study on microstructure and tensile behaviour of a selectively laser melted stainless steel, Sci Rep 8 (2018). https://doi.org/10.1038/s41598-018-26136-7.

[84] R. Michel, Y. Bienvenu, A. Chesnaud, A. Thorel, Study of the tensile behaviour of tungsten wires from ambient temperature to 320 °C in relation to their microstructure, Int J Refract Metals Hard Mater 92 (2020). https://doi.org/10.1016/j.ijrmhm.2020.105325.

[85] S. Sinha, A. Ghosh, N.P. Gurao, Effect of initial orientation on the tensile properties of commercially pure titanium, Philosophical Magazine 96 (2016). https://doi.org/10.1080/14786435.2016.1165873.

[86] Q. Chen, X. Wang, F. Chen, N. Zhang, M. Ma, Extremely strong and tough polythiophene composite for flexible electronics, Chemical Engineering Journal 368 (2019). https://doi.org/10.1016/j.cej.2019.02.203.

[87] L. Huang, L. Wang, M. Qian, J. Zou, High tensile-strength and ductile titanium matrix composites strengthened by TiB nanowires, Scr Mater 141 (2017). https://doi.org/10.1016/j.scriptamat.2017.08.007.

[88] M. Alves, D. Carlstedt, F. Ohlsson, L.E. Asp, S. Pimenta, Ultra-strong and stiff randomly-oriented discontinuous composites: Closing the gap to quasi-isotropic continuous-fibre laminates, Compos Part A Appl Sci Manuf 132 (2020). https://doi.org/10.1016/j.compositesa.2020.105826.

[89] Fibre–polymer composites for aerospace structures and engines, in: Introduction to Aerospace Materials, 2012. https://doi.org/10.1533/9780857095152.338.

[90] O.K. Park, H. Choi, H. Jeong, Y. Jung, J. Yu, J.K. Lee, J.Y. Hwang, S.M. Kim, Y. Jeong, C.R. Park, M. Endo, B.C. Ku, High-modulus and strength carbon nanotube fibers using molecular cross-linking, Carbon 118 (2017). https://doi.org/10.1016/j.carbon.2017.03.079.

[91] Y.N. Liu, M. Li, Y. Gu, K. Wang, D. Hu, Q. Li, Z. Zhang, A modified spray-winding approach to enhance the tensile performance of array-based carbon nanotube composite films, Carbon 65 (2013). https://doi.org/10.1016/j.carbon.2013.08.013.

[92] M.S. Wang, D. Golberg, Y. Bando, Tensile tests on individual single-walled carbon nanotubes: Linking nanotube strength with its defects, Advanced Materials 22 (2010). https://doi.org/10.1002/adma.201001463.

[93] M.F. Yu, O. Lourie, M.J. Dyer, K. Moloni, T.F. Kelly, R.S. Ruoff, Strength and breaking mechanism of multiwalled carbon nanotubes under tensile load, Science (1979) 287 (2000). https://doi.org/10.1126/science.287.5453.637.

[94] C. Lee, X. Wei, J.W. Kysar, J. Hone, Measurement of the elastic properties and intrinsic strength of monolayer graphene, Science (1979) 321 (2008). https://doi.org/10.1126/science.1157996.

[95] R. Kotsilkova, I. Borovanska, P. Todorov, E. Ivanov, D. Menseidov, S. Chakraborty, C. Bhattacharjee, Tensile and Surface Mechanical Properties of Polyethersulphone (PES) and Polyvinylidene Fluoride (PVDF) Membranes, Journal of Theoretical and Applied Mechanics (Bulgaria) 48 (2018). https://doi.org/10.2478/jtam-2018-0018.

[96] F. Fallah, M. Khorasani, M. Ebrahimi, Improving the mechanical properties of waterborne nitrocellulose coating using nano-silica particles, Prog Org Coat 109 (2017). https://doi.org/10.1016/j.porgcoat.2017.04.016.

[97] F.C.P. Sales, R.M. Ariati, V.T. Noronha, J.E. Ribeiro, Mechanical characterization of PDMS with different mixing ratios, in: Procedia Structural Integrity, 2021. https://doi.org/10.1016/j.prostr.2022.01.099.

[98] S.D. Shandakov, A. V. Kosobutsky, A.I. Vershinina, O.G. Sevostyanov, I.M. Chirkova, D.M. Russakov, M. V. Lomakin, M.S. Rybakov, T. V. Glushkova, E.A. Ovcharenko, M.A. Zhilyaeva, A.G. Nasibulin, Electromechanical properties of fibers produced from randomly oriented SWCNT films by wet pulling technique, Materials Science and Engineering: B 269 (2021). https://doi.org/10.1016/j.mseb.2021.115178.

[99] M.A. Zhilyaeva, E. V. Shulga, S.D. Shandakov, I. V. Sergeichev, E.P. Gilshteyn, A.S. Anisimov, A.G. Nasibulin, A novel straightforward wet pulling technique to fabricate carbon nanotube fibers, Carbon 150 (2019) 69–75. https://doi.org/10.1016/j.carbon.2019.04.111.

[100] H. Zhan, Y.W. Chen, Q.Q. Shi, Y. Zhang, R.W. Mo, J.N. Wang, Highly aligned and densified carbon nanotube films with superior thermal conductivity and mechanical strength, Carbon 186 (2022) 205–214. https://doi.org/10.1016/j.carbon.2021.09.069.

[101] F. Peng, Y. Jiang, J. Feng, L. Li, H. Cai, J. Feng, A facile method to fabricate monolithic alumina–silica aerogels with high surface areas and good mechanical properties, J Eur Ceram Soc 40 (2020). https://doi.org/10.1016/j.jeurceramsoc.2020.01.058.

[102] A. Perez-Moreno, M. de las V. Reyes-Peces, D.M. de los Santos, G. Pinaglia-Tobaruela, E. de la Orden, J.I. Vilches-Pérez, M. Salido, M. Piñero, N. de la Rosa-Fox, Hydroxyl groups induce bioactivity in silica/chitosan aerogels designed for bone tissue engineering. In vitro model for the assessment of osteoblasts behavior, Polymers (Basel) 12 (2020). https://doi.org/10.3390/polym12122802.

[103] H. Maleki, M.A. Shahbazi, S. Montes, S.H. Hosseini, M.R. Eskandari, S. Zaunschirm, T. Verwanger, S. Mathur, B. Milow, B. Krammer, N. Hüsing, Mechanically Strong Silica-Silk Fibroin Bioaerogel: A Hybrid Scaffold with Ordered Honeycomb Micromorphology and Multiscale Porosity for Bone Regeneration, ACS Appl Mater Interfaces 11 (2019). https://doi.org/10.1021/acsami.9b04283.

[104] S. Long, Y. Feng, F. He, S. He, H. Hong, X. Yang, L. Zheng, J. Liu, L. Gan, M. Long, An ultralight, supercompressible, superhydrophobic and multifunctional carbon aerogel with a specially designed structure, Carbon 158 (2020). https://doi.org/10.1016/j.carbon.2019.11.065.

[105] F. Guo, Y. Jiang, Z. Xu, Y. Xiao, B. Fang, Y. Liu, W. Gao, P. Zhao, H. Wang, C. Gao, Highly stretchable carbon aerogels, Nat Commun 9 (2018). https://doi.org/10.1038/s41467-018-03268-y.

[106] P. Nautiyal, C. Zhang, A. Loganathan, B. Boesl, A. Agarwal, High-Temperature Mechanics of Boron Nitride Nanotube "Buckypaper" for Engineering Advanced Structural Materials, ACS Appl Nano Mater 2 (2019) 4402–4416. https://doi.org/10.1021/acsanm.9b00817.

[107] M.B. Jakubinek, B. Ashrafi, J. Guan, M.B. Johnson, M.A. White, B. Simard, 3D chemically cross-linked single-walled carbon nanotube buckypapers, RSC Adv. 4 (2014) 57564–57573. https://doi.org/10.1039/C4RA12026D.

[108] S. Upama, L. Arevalo, A. Pendashteh, A. Mikhalchan, M.J. Green, J.J. Vilatela, Joule Heating in Controlled Atmospheres to Process Nanocarbon/Transition Metal Oxide Composites and Electrodes, ACS Appl Nano Mater (2024). https://doi.org/10.1021/acsanm.4c02081.

Declaration of interests

☒ The authors declare that they have no known competing financial interests or personal relationships that could have appeared to influence the work reported in this paper.

☐ The authors declare the following financial interests/personal relationships which may be considered as potential competing interests: